Title	Comparison of various methods for quantification of apparent diffusion coefficient of head and neck lesions with HASTE diffusion-weighted MR imaging
Author(s) Alternative	Sakamoto, J; Sasaki, Y; Otonari-Yamamoto, M; Sano, T
Journal	Oral surgery, oral medicine, oral pathology and oral radiology, 114(2): 266-276
URL	http://hdl.handle.net/10130/2936
Right	

Comparison of various methods for quantification of ADC of head and neck lesions with HASTE diffusion-weighted MR imaging

Junichiro SAKAMOTO, DDS, Ph.D*, Yoshinori SASAKI DDS,
Mika OTONARI-YAMAMOTO, DDS, Ph.D, Tsukasa SANO, DDS, Ph.D.

Department of Oral and Maxillofacial Radiology, Tokyo Dental College,
1-2-2 Masago, Mihama-ku, Chiba-shi, Chiba
261-8502, Japan.
*: Corresponding author.
Tel.: +81 43 270 3961; fax: +81 43 270 3963.
E-mail address: sakamotojun@tdc.ac.jp

Acknowledgments

This study was supported by KAKENHI (40506896). We would like to thank Associate Professor Jeremy Williams, Tokyo Dental College, for his assistance with the English of this manuscript.

Conflict of interest

Each author certifies that he or she has no commercial associations that might pose a conflict of interest in connection with this manuscript.

Word count for the manuscript: 3562 words (Abstract: 139 words)
Number of tables: 5 tables
Number of figures: 7 figures
Number of references: 25 references

Abstract

Objectives. The purposes of this retrospective study were to compare various methods of apparent diffusion coefficient (ADC) measurement for head and neck lesions in half-Fourier single-shot turbo spin-echo (HASTE) diffusion-weighted imaging (DWI) and determine the threshold ADC value for predicting malignancy.

Study Design. HASTE DW images of 46 lesions (10 cysts, 14 benign tumors, and 22 malignant tumors) were studied retrospectively. The ADC values were compared between 0-1000 method, 500-1000 method, and weighted linear regression (WLR) fit.

Results. The highest overall accuracies of 83.3%, 86.1%, and 88.9% were obtained when ADC values of 1.24×10^{-3} mm^2/sec (0-1000 method), 0.98×10^{-3} mm^2/sec (500-1000 method), and 1.23×10^{-3} mm^2/sec (WLR fit), respectively, were used for the threshold.

Conclusions. The present results indicate that ADC measurement with HASTE DWI is useful in predicting malignancy of head and neck lesions.

Introduction

Preoperative diagnosis of head and neck lesions is important in surgical planning, and predicting malignancies in the head and neck region, in particular, is essential not only for surgical planning, but also prognosis. Several imaging techniques, including computed tomography, ultrasound, magnetic resonance imaging (MRI), and positron emission tomography can be helpful in diagnosing head and neck lesions. Recently, a number of MRI techniques have been developed that provide functional information which can be used to evaluate head and neck lesions[1].

Diffusion-weighted imaging (DWI) allows visualization of microscopic water diffusion in biological tissues[2-5], and has been applied to head and neck lesions. Many researchers have applied echo-planar imaging (EPI) to DWI of head and neck lesions, as well as diagnosis of diseases of the central nerve system. However, EPI in the head and neck region has several inherent drawbacks, being affected by susceptibility, chemical shift, and N/2 artifacts[6-13]. An alternative to EPI, fast spin-echo DWI, is currently under investigation. One of these techniques is half-Fourier single-shot turbo spin-echo (HASTE), also known as single-shot fast spin echo or fast asymmetric spin

echo (FASE). The advantage of this technique over EPI is that it is relatively unaffected by susceptibility, chemical shift or N/2 artifacts.

One method of evaluating DWI is to measure the apparent diffusion coefficient (ADC), and several researchers have reported the usefulness of this technique in the evaluation of head and neck lesions[7-19]. The ADC can be useful in characterizing both normal and pathological tissue as it reflects microscopic water diffusion and tissue perfusion in biologic tissues[2-5]. In many studies, linear regression and gradient b factors of 0 and 1000 sec/mm^2 have been applied to ADC measurement[7-9,11-14,17,18]. However, other gradient b factors have also been used for ADC measurement[8,10,15,16,19]. Therefore, as yet, no consensus exists regarding the optimum gradient b factors and methods to be applied to ADC measurement. At our institution, HASTE DWI and linear regression with gradient b factors of 0 and 1000 sec/mm^2 for ADC measurement are used. In addition, a threshold ADC value of 1.10 × 10^{-3} mm^2/sec has been used to predict malignancy in reference to earlier studies. However, it has been suggested that the threshold ADC value for predicting malignancy should be determined according to each MR system, as MR units, pulse sequences, and

operation of units may vary[9]. As far as we know, no studies to date have compared the various methods of ADC measurement for head and neck lesions with HASTE DWI in order to determine the threshold ADC value for predicting malignancy.

The purposes of this retrospective study were to compare various methods of ADC measurement for head and neck lesions in HASTE DWI and determine the threshold ADC value for predicting malignancy at our institution.

Materials and methods

Patients

A total of 72 patients with head and neck mass lesions who visited our hospital between January and November 2010 underwent conventional MRI and DWI. Among them, 28 patients were excluded from this study due to a lack of a final diagnosis in 22, an absence of a small mass lesion on conventional MR images in 5 with squamous cell carcinoma, and image distortion because of motion artifact on the DW images in one child. Therefore, a total of 44 patients with 46 head and neck lesions were included in this retrospective study. The patients comprised 19 men and 25 women with a mean age of 55.1 years (range, 20-79 years). In 34 of the 46 lesions, the final diagnoses were made histologically by using either surgery or biopsy. Among the remaining 12 cases, the diagnoses of five ranulas, two retention cysts, and five vascular malformations were established by their characteristic clinical and MR findings. The lesions were divided into 10 cysts, 14 benign tumors, and 22 malignant tumors, as shown in Table 1. Informed consent was obtained from all patients, and the study protocol was approved by our institutional review board (No. 314).

MRI Techniques

A 1.5-T whole-body MR system (Magnetom Symphony Maestro Class, Siemens, Erlangen, Germany) and head and neck coil were used to obtain all MR images. The standard MRI protocol for head and neck lesions at our institution includes The standard MRI protocol for head and neck lesions at our institution includes T1-weighted spin-echo images (TR [msec] / TE [msec] =500/15; number of signal averaged [NSA] = 1) in the axial and coronal planes, and T2-weighted turbo spin-echo imaging (TR/TE = 4600/90; TI = 110 msec; turbo factor = 19; NSA = 1) with the fat suppression by short inversion time inversion-recovery and chemical-shift selective saturation (Dual-FS-STIR- CHESS) in the axial and coronal planes[20].

T1-weighted and T2-weighted images were obtained with a matrix of 384 × 384 for T1-weighted images and 320 × 320 for T2-weighted images, a FOV of 230 × 230 mm, and a section thickness of 4-6 mm with an intersection gap of 0.8-1.2 mm.

If the lesions were depicted onT1-weighted or T2-weighted images, HASTE DW images (TR/TE = 3000/101; receiver bandwidth [RBW] = 630 Hz/pixel; NSA = 1) were obtained in the axial plane at the section where the diameter of the lesion shown

was largest, with a matrix of 192 × 192, a FOV of 230 × 230 mm, and a section thickness of 4-5 mm with an intersection gap of 0.8-1.0 mm.

Motion-probing gradients were applied in each of the three orthogonal directions, with six values for the gradient b factors of 0, 100, 300, 500, 700, and 1000 sec/mm^2. After HASTE DWI in 26 patients, T1-weighted spin-echo images (TR/TE = 500/15; NSA = 1) with fat suppression by CHESS were also obtained in the axial and coronal planes after intravenous administration of 0.1 mmol/kg meglumine gadoterate (Magnescope, Guerbet Japan, Tokyo, Japan), with a matrix of 384 × 384, a FOV of 230 × 230 mm, a section thickness of 4-6 mm, and an intersection gap of 0.8-1.2 mm.

MR imaging analysis

In the linear regression model, ADC was obtained according to the following equation:

$$\text{ADC } (\text{mm}^2/\text{sec}) = -[1/(b_2 - b_1)] \ln (SI_2/SI_1), \text{-(1)}$$

where SI_1 and SI_2 are the signal intensities measured at a lower gradient b factor (b_1) and a higher gradient b factor (b_2). Therefore, the ADC values were calculated with a set of gradient b factors of 0 and 1000 sec/mm^2 (0-1000 method) and another set of 500 and

1000 sec/mm^2 (500-1000 method) for each lesion. Furthermore, the equation above (1) is based on a general mathematical model describing signal decaying processes which assumes mono-exponential decay under the presence of the motion-proving gradients[21]. Therefore, a weighted linear regression fit (WLR fit) was also performed to calculate ADC values. A circular region of interest (ROI) was placed on the DW images using T1-weighted, T2-weighted, or contrast-enhanced T1-weighted images as reference images. One oral radiologist (Y.S.) placed ROI using electric cursor on the DW images with special attention to avoiding over or under estimation. The placed ROIs were checked by consensus of two experienced oral radiologists (J.S. and M.O-Y.) for each patient. Furthermore, ADC maps were constructed from HASTE DW images with gradient b factors of 0 and 1000 sec/mm^2. Image processing was performed using the operator console of the MR system.

Statistical analysis

A one-way analysis of variance (one-way ANOVA) and multiple comparison (Tukey-Kramer) test were used to detect significant differences among the mean ADC values for the three categories in each method: 0-1000 method, 500-1000 method, and

WLR fit, respectively. A receiver operating characteristics (ROC) curve was also used to evaluate diagnostic ability of ADC value for differentiating malignant tumors from benign tumors among the three methods. A *P* value of less than 0.05 was considered statistically significant. Furthermore, sensitivity, specificity, accuracy, positive predictive value and negative predictive value were also calculated to determine the most suitable threshold ADC value for predicting malignancy in each method. Analyses were performed with the statistical software package R version 2.12.0 for Windows(R Development Core Team, Vienna, Austria)[22] and DBM MRMC 2.2 Build 3(Medical Image Perception Laboratory, Iowa, USA)[23].

Results

The mean ADC values for the cysts, benign and malignant tumors with each method were shown in Table 2. The mean ADC value of the cysts was the highest, followed by those of benign and malignant tumors with each method, and there were significant differences in the mean ADC values among the three categories with each method (one-way ANOVA: $P < 0.05$; Tukey-Kramer test: $P < 0.05$). Fig. 1 shows box plots of the ADC values obtained with each method.

Fig. 2 shows the ROC curves of diagnostic ability of ADC value for the differentiating malignant from benign tumors among the three methods. The areas under the ROC curves (AUCs) were 0.844 ± 0.0806 (95% confidence interval: 0.680 - 1.08) with 0-1000 method, 0.902 ± 0.0663 (95% confidence interval: 0.767 - 1.04) with 500-1000 method, and 0.867 ± 0.0832 (95% confidence interval: 0.698 - 1.04) with WLR fit. No significant difference was observed among the AUCs of all three methods ($P > 0.05$). Tables 3-5 show statistical data for predicting malignancy in each method. The highest overall accuracies of 83.3%, 86.1%, and 88.9% were obtained when ADC values of 1.24×10^{-3} mm^2/sec with 0-1000 method, 0.98×10^{-3} mm^2/sec with 500-1000

method, and 1.23×10^{-3} mm^2/sec with WLR fit, respectively, were used for the threshold. Representative cases are shown in Figs. 3-7.

Discussion

In this study, we used HASTE DWI, a fast spin-echo DWI technique. Several studies on the application of this technique to other regions such as the brain, spinal cord, and breast reported that the usefulness of this technique was limited and inferior to that of EPI[5,24,25]. Kito et al.[13], however, reported that many kinds of tissues in the oral and maxillofacial regions were relatively well visualized in all subjects on FASE DWI (HASTE DWI), but not well on EPI. They concluded that FASE DWI might be useful in the detection of abscess formation in the oral and maxillofacial regions. Other studies have investigated the usefulness of split acquisition of fast spin-echo signals for diffusion-weighted imaging (SPLICE), a modified HASTE technique, in the evaluation of head and neck lesions[11,12]. Yoshino et al.[11] reported that DW images and ADC maps of the salivary gland had higher quality with SPLICE rather than with EPI. In this study, reliable HASTE DW images and ADC values were obtained, even when the lesion was relatively small, as shown in Figs. 3 and 5. In addition, the HASTE DW images showed little susceptibility to artifact due to dental restorations, as shown in Fig. 7. This technique utilizes refocusing radio frequency pulses instead of gradient rephrasing,

which is utilized for EPI and results in magnetic susceptibility distortions[6,11,13]. Thus, HASTE DW images have less affect of susceptibility artifacts than EPI. Especially, in the head and neck, susceptibility distortions tend to occur because of the presence of numerous dental restorations and anatomical air spaces existing there. This advantage might contribute much to obtaining the reliable HASTE DW images and ADC values. Furthermore, high image resolution might also contribute to the depiction of the relatively small lesions on the HASTE DW images because a number of small organs are tightly packed together within the head and neck, and mass lesions occurring in this area tend to be small. These results agree with these earlier studies, indicating that HASTE DWI is useful in the evaluation of head and neck lesions.

Many earlier studies employing ADC measurement have used the linear regression model and various sets of gradient b factors[6-16,18,19]. This model was also applied in this study, and three sets of gradient b factors (0 and 1000 sec/mm^2, 500 and 1000 sec/mm^2, and all b factors for WLR fit) were compared. The mean ADC value of the cysts was the highest, followed by that of benign tumors and that of malignant tumors, regardless of the measurement method used. These results are compatible with

those of previous studies[7-9,11-13,19]. The mobility of water molecules in fluid is freer than that in solid biological tissues, and the ADC values of cysts are higher than those of benign or malignant tumors[8,9,12]. On the other hand, the histopathological characteristics of malignant tumors such as enlarged nuclei, hyper-chromatism, and hypercellularity, reduce the extracellular matrix and the diffusion space of water molecules[7-9,11-13,15,16,18]. As a result, the ADC values of benign tumors are higher than those of malignant tumors. However, one dermoid cyst showed markedly low ADC values of 0.908×10^{-3} mm^2/sec with 0-1000 method, 0.990×10^{-3} mm^2/sec with 500-1000 method, and 0.880×10^{-3} mm^2/sec with WLR fit in this study. It was confirmed histopathologically that this dermoid cyst contained keratinous debris and had a very thick wall. Higher protein content in a fluid might increase viscosity and decrease the mobility of water molecules[8,12]. In addition, a thick wall might contribute to a decrease in ADC values. It was also observed that the mean ADC value with 500-1000 method was slightly lower than those with the remaining methods in all categories. This may have been due to a reduction in the contribution of tissue perfusion such as microcirculation of the blood in the capillary network in tissues with a high gradient b factor of 500 or 1000 sec/mm^2 [8,9].

In this study, high overall accuracies were obtained for predicting malignancy and no significant difference was observed among diagnostic abilities of all three methods. This indicates that HASTE DWI of head and neck lesions is useful in predicting malignancy with a linear regression model, regardless of the set of gradient b factors. Wang et al.[9] used EPI in the evaluation of the head and neck lesions and reported that when an ADC value of 1.22×10^{-3} mm^2/s or less was used for predicting malignancy, the accuracy was 86%, with 84% sensitivity, and 91% specificity. Razek et al.[19] also used EPI in the evaluation of the pediatric head and neck masses and obtained the accuracy of 92.8% for differentiating malignant from benign head and neck mass. The accuracies of this study were equivalent to or slightly less than these earlier studies. On the other hand, Sakamoto et al.[12] reported that ADC values with SPLICE contributed little in predicting malignancy. Although this discrepancy with the current results may have been due to differences in the case series, we believe that optimization of imaging parameters was probably responsible for the favorable outcome observed in the present study. In our MR system, more specific imaging parameters such as RBW and echo space are adjustable, and to improve HASTE DWI for head and neck lesions,

a wider RBW, shorter echo space, and relatively lower matrix than other conventional MRI are used. Among the three methods used in the current study, we believe that 0-1000 or 500-1000 method would be the most appropriate in clinical practice, as they are concise procedures involving a shorter scan time than WLR fit.

There were several limitations to this study, the first being that the sample was relatively small. Moreover, several types of cyst and tumor can occur in the head and neck region. Therefore, further study is necessary to validate these results. Secondly, HASTE DW MR imaging has a number of drawbacks such as severe blurring and a low signal-to-noise ratio (SNR). As mentioned above, however, severe blurring was decreased by optimizing the imaging parameters. A low SNR, however, could not be avoided altogether. Therefore, the depiction of the lesions was not clear in some cases. This indicates the need to improve the low SNR by some means, perhaps by increasing NSA.

In conclusion, pathological tissues were characterized effectively by ADC with HASTE DWI. High overall accuracies were obtained for predicting malignancy when suitable ADC values were used for the threshold. These results indicate that ADC

measurement with HASTE DWI is useful in predicting malignancy of head and neck lesions.

References

[1] Alberico RA, Husain SH, Sirotkin I. Imaging in head and neck oncology. Surg Oncol Clin N Am 2004;13:13-35.

[2] Le Bihan D, Breton E, Lallemand D, Grenier P, Cabanis E, Laval-Jeantet M. MR imaging of intravoxel incoherent motions: application to diffusion and perfusion in neurologic disorders. Radiology 1986;161:401-7.

[3] Turner R, Le Bihan D, Maier J, Vavrek R, Hedges LK, Pekar J. Echo-planar imaging of intravoxel incoherent motion. Radiology 1990;177:407-14.

[4] Muller MF, Prasad P, Siewert B, Nissenbaum MA, Raptopoulos V, Edelman RR. Abdominal diffusion mapping with use of a whole-body echo-planar system. Radiology 1994;190:475-8.

[5] Schaefer PW, Grant PE, Gonzalez RG. Diffusion-weighted MR imaging of the brain. Radiology 2000;217:331-45.

[6] Lovblad KO, Jakob PM, Chen Q, Baird AE, Schlaug G, Warach S, et al. Turbo spin-echo diffusion-weighted MR of ischemic stroke. AJNR American journal of neuroradiology 1998;19:201-8.

[7] Chawla S, Kim S, Wang S, Poptani H. Diffusion-weighted imaging in head and neck cancers. Future Oncol 2009;5:959-75.

[8] Razek AA. Diffusion-weighted magnetic resonance imaging of head and neck. J Comput Assist Tomogr 2010;34:808-15.

[9] Wang J, Takashima S, Takayama F, Kawakami S, Saito A, Matsushita T, et al. Head and neck lesions: characterization with diffusion-weighted echo-planar MR imaging. Radiology 2001;220:621-30.

[10] Maeda M, Kato H, Sakuma H, Maier SE, Takeda K. Usefulness of the apparent diffusion coefficient in line scan diffusion-weighted imaging for distinguishing between squamous cell carcinomas and malignant lymphomas of the head and neck. AJNR Am J Neuroradiol 2005;26:1186-92.

[11] Yoshino N, Yamada I, Ohbayashi N, Honda E, Ida M, Kurabayashi T, et al. Salivary glands and lesions: evaluation of apparent diffusion coefficients with split-echo diffusion-weighted MR imaging--initial results. Radiology 2001;221:837-42.

[12] Sakamoto J, Yoshino N, Okochi K, Imaizumi A, Tetsumura A, Kurohara K, et al. Tissue characterization of head and neck lesions using diffusion-weighted MR

imaging with SPLICE. Eur J Radiol 2009;69:260-8.

[13] Kito S, Morimoto Y, Tanaka T, Tominaga K, Habu M, Kurokawa H, et al. Utility of diffusion-weighted images using fast asymmetric spin-echo sequences for detection of abscess formation in the head and neck region. Oral Surg Oral Med Oral Pathol Oral Radiol Endod 2006;101:231-8.

[14] Yabuuchi H, Matsuo Y, Kamitani T, Setoguchi T, Okafuji T, Soeda H, et al. Parotid gland tumors: can addition of diffusion-weighted MR imaging to dynamic contrast-enhanced MR imaging improve diagnostic accuracy in characterization? Radiology 2008;249:909-16.

[15] Sumi M, Sakihama N, Sumi T, Morikawa M, Uetani M, Kabasawa H, et al. Discrimination of metastatic cervical lymph nodes with diffusion-weighted MR imaging in patients with head and neck cancer. AJNR Am J Neuroradiol 2003;24:1627-34.

[16] Eida S, Sumi M, Sakihama N, Takahashi H, Nakamura T. Apparent diffusion coefficient mapping of salivary gland tumors: prediction of the benignancy and malignancy. AJNR American journal of neuroradiology 2007;28:116-21.

[17] Juan CJ, Chang HC, Hsueh CJ, Liu HS, Huang YC, Chung HW, et al.

Salivary glands: echo-planar versus PROPELLER Diffusion-weighted MR imaging for assessment of ADCs. Radiology 2009;253:144-52.

[18] Wang P, Yang J, Yu Q, Ai S, Zhu W. Evaluation of solid lesions affecting masticator space with diffusion-weighted MR imaging. Oral Surg Oral Med Oral Pathol Oral Radiol Endod 2010;109:900-7.

[19] Razek AA, Gaballa G, Elhawarey G, Megahed AS, Hafez M, Nada N. Characterization of pediatric head and neck masses with diffusion-weighted MR imaging. Eur Radiol 2009;19:201–8.

[20] Tanabe K, Nishikawa K, Sano T, Sakai O, Jara H. Fat suppression with short inversion time inversion-recovery and chemical-shift selective saturation: a dual STIR-CHESS combination prepulse for turbo spin echo pulse sequences. J Magn Reson Imaging 2010;31:1277-81.

[21] Papanikolaou N, Gourtsoyianni S, Yarmenitis S, Maris T, Gourtsoyiannis N. Comparison between two-point and four-point methods for quantification of apparent diffusion coefficient of normal liver parenchyma and focal lesions. Value of normalization with spleen. Eur J Radiol 2010;73:305-9.

[22] R Development Core Team. R: a language and environment for statistical computing. Vienna, Austria: R Foundation for Statistical Computing; 2010. Available at: http://www.r-project.org/. Accessed

[23] Dorfman DD, Berbaum KS, Metz CE. Receiver operating characteristic rating analysis. Generalization to the population of readers and patients with the jackknife method. Invest Radiol 1992;27:723-31.

[24] Baltzer PA, Renz DM, Herrmann KH, Dietzel M, Krumbein I, Gajda M, et al. Diffusion-weighted imaging (DWI) in MR mammography (MRM): clinical comparison of echo planar imaging (EPI) and half-Fourier single-shot turbo spin echo (HASTE) diffusion techniques. European radiology 2009;19:1612-20.

[25] Bammer R, Augustin M, Prokesch RW, Stollberger R, Fazekas F. Diffusion-weighted imaging of the spinal cord: interleaved echo-planar imaging is superior to fast spin-echo. J Magn Reson Imaging 2002;15:364-73.

Legends.

Fig. 1.

Box plots of ADC values with 0-1000 method (light gray boxes), 500-1000 method (gray boxes), and weighted linear regression (WLR) fit (white boxes) among three categories. Highest mean ADC value was that for cysts, followed by that for benign and malignant tumors with each method.

Fig. 2.

ROC curves of diagnostic ability for predicting malignancy among three methods for ADC measurement. Solid line indicates ROC curve with 0-1000 method; dashed line indicates that with 500-1000 method; dotted line indicates that with WLR fit.

Fig. 3.

Ranula in left sublingual space in 20-year-old woman. (a)-(b) **Axial** and coronal **T2-weighted images** revealed mass lesion with homogeneous, very high signal intensity. (c) **HASTE DW image** obtained with gradient b factor of 0 sec/mm^2 revealed

mass lesion with very high signal intensity. (d)-(e) **HASTE DW image**s obtained with gradient b factors of 500 and 1000 sec/mm^2 showed marked decrease in signal intensity of mass lesion. (f) ADC map shows that mass lesion had high ADC value of 2.09 × 10^{-3} mm^2/sec with 0-1000 method, 1.73 × 10^{-3} mm^2/sec with 500-1000 method, and 2.13 × 10^{-3} mm^2/sec with WLR fit. This case was correctly diagnosed as a non-malignancy using threshold ADC values with each method.

Fig. 4.

Myoepithelioma in right palate in 50-year-old woman. (a) **Axial T2-weighted image** revealed mass lesion (arrowhead) with heterogeneous, very high signal intensity. (b) **Axial post-contrast T1-weighted image** showed mass lesion was enhanced strongly. (c) **HASTE DW image** obtained with gradient b factor of 0 sec/mm^2 revealed mass lesion (arrowhead) with very high signal intensity. (d)-(e) **HASTE DW image**s obtained with gradient b factors of 500 and 1000 sec/mm^2 showed mild decrease in signal intensity of mass lesion. (f) ADC map shows that mass lesion had an ADC value of 1.54 × 10^{-3} mm^2/sec with 0-1000 method, 1.38 × 10^{-3} mm^2/sec with 500-1000 method,

and 1.67×10^{-3} mm^2/sec with WLR fit. Whereas it is a little difficult to diagnose a mass lesion as a benign tumor using only conventional MR images, ADC values with **HASTE DWI** were very helpful in differentiating non-malignancy from malignancy in this case. This case was correctly diagnosed as a non-malignancy using threshold ADC values with each method.

Fig. 5.

Cavernous hemangioma in right buccal space in 58-year-old woman. (a) **Axial T2-weighted image** revealed relatively small mass lesion with homogenous, very high signal intensity. (b) **Axial post-contrast T1-weighted image** showed mass lesion was enhanced strongly. (c) **HASTE DW image** obtained with gradient b factor of 0 sec/mm^2 revealed mass lesion with very high signal intensity. (d)-(e) **HASTE DW image**s obtained with gradient b factors of 500 and 1000 sec/mm^2 showed mild decrease in signal intensity of mass lesion. (f) ADC map shows that mass lesion had an ADC value of 1.46×10^{-3} mm^2/sec with 0-1000 method, 1.10×10^{-3} mm^2/sec with 500-1000 method, and 1.45×10^{-3} mm^2/sec with WLR fit. This case was also correctly diagnosed as a

non-malignancy using threshold ADC values with each method.

Fig. 6.

Malignant lymphoma in palate of 72-year-old woman. (a) **Axial** T1-weighted image revealed mass lesion with homogeneous, low signal intensity. (b) **Axial T2-weighted image** revealed mass lesion with homogeneous, slightly high signal intensity. (c) **HASTE DW image** obtained with gradient b factor of 0 sec/mm^2 revealed mass lesion with slightly high signal intensity. (d)-(e) **HASTE DW image**s obtained with gradient b factors of 500 and 1000 sec/mm^2 showed slight decrease in signal intensity of mass lesion. (f) ADC map shows that mass lesion had relatively lower ADC value of 0.61 × 10^{-3} mm^2/sec with 0-1000 method, 0.49× 10^{-3} mm^2/sec with 500-1000 method, and 0.59 × 10^{-3} mm^2/sec with WLR fit. This case was correctly diagnosed as a malignancy using threshold ADC values with each method.

Fig. 7.

Squamous cell carcinoma in right tongue of 46-year-old woman. (a) **Axial T2-weighted**

image revealed mass lesion with high signal intensity. Susceptibility artifacts due to dental restorations (arrowheads) are shown on images. (b) **Axial post-contrast T1-weighted image** showed mass lesion was enhanced. Susceptibility artifacts due to dental restorations (arrowheads) are also shown on images. (c) **HASTE DW image** obtained with gradient b factors of 0 sec/mm^2 revealed mass lesion with slightly high signal intensity. Although susceptibility artifacts due to dental restorations were present on this image, as well as on **T2-weighted** and **post-contrast T1-weighted images**, no distortion severe enough to hamper ADC measurement was observed. (d)-(e) **HASTE DW image**s obtained with gradient b factors of 500 and 1000 sec/mm^2 showed slight decrease in signal intensity of mass lesion. (f) ADC map shows that mass lesion had low ADC value of 1.00×10^{-3} mm^2/sec with 0-1000 method, 0.69×10^{-3} mm^2/sec with 500-1000 method, and 0.96×10^{-3} mm^2/sec with WLR fit. This case was also correctly diagnosed as a malignancy using threshold ADC values with each method.

Table 1. Diagnosis and location of 46 head and neck lesions

Category	Diagnosis	Location
Cyst (n = 10)	Dermoid cyst (n = 1)	Oral cavity
	Ranula (n = 7)	Submadibular and/or sublingual space
	Retention cyst (n = 2)	Maxillary sinus
Benign tumor (n = 14)	Ancient shwannoma (n = 1)	Palate
	Intraductal papilloma (n = 1)	Palate
	Myoepithelioma (n = 1)	Palate
		Palate
	Pleomorphic adenoma (n = 3)	Upper lip
		Submandibular gland
	Vascular malformation (n = 8)	Oral cavity (n = 2)
		Buccal space (n = 2)
		Lower lip
		Submandibular space (n = 2)
		Parotid gland
Malignant tumor (n = 22)	Carcinoma ex pleomorphic adenoma (n = 1)	Palate
	Malignant lymphoma (n = 1)	Palate
	Squamous cell carcinoma (n = 19)	Oral cavity
	Verrucous carcinoma (n = 1)	Oral cavity

Data in parentheses are the number of cases

Table 2. Mean ADC values of the head and neck Lesions

Categories	0-1000 method*	500-1000 method*	WLR fit*
Cysts	2.21 ± 0.52	1.87 ± 0.39	2.21 ±0.53
Benign tumors	1.39 ± 0.33	1.11 ± 0.27	1.40 ± 0.39
Malignant tumors	1.02 ± 0.02	0.65 ± 0.23	0.99 ± 0.22

A one-way ANOVA and Tukey-Kramer test were used to detect significant differences among the mean ADC values for the three categories in each method.

ADC values are expressed as the (mean ± SD) $\times 10^{-3}$ mm^2/sec.

*** One-way ANOVA: $P < 0.05$; Tukey-Kramer test: $P < 0.05$**

Table 3. Statistical data for the predicting malignancy with 0-1000 method

Threshold value of ADC ($\times 10^{-3}$ mm^2/sec)	Sensitivity (%)	Specificity (%)	Accuracy (%)	PPV (%)	NPV (%)
≦1.22	81.8 (18/22)	78.6 (11/14)	80.6 (29/36)	85.7 (18/21)	73.3 (11/15)
≦1.23	81.8 (18/22)	78.6 (11/14)	80.6 (29/36)	85.7 (18/21)	73.3 (11/15)
≦1.24	**86.4 (19/22)**	**78.6 (11/14)**	**83.3 (30/36)**	**86.4 (19/22)**	**78.6 (11/14)**
≦1.25	86.4 (19/22)	78.6 (11/14)	83.3 (30/36)	86.4 (19/22)	78.6 (11/14)
≦1.26	86.4 (19/22)	78.6 (11/14)	83.3 (30/36)	86.4 (19/22)	78.6 (11/14)

Data in parentheses are the number of cases used to calculate the percentages.

Table 4. Statistical data for the predicting malignancy with 500-1000 method

Threshold value of ADC ($\times 10^{-3}$ mm^2/sec)	Sensitivity (%)	Specificity (%)	Accuracy (%)	PPV (%)	NPV (%)
≦0.96	90.9 (20/22)	78.6 (11/14)	86.1 (31/36)	87.0 (20/23)	84.6 (11/13)
≦0.97	90.9 (20/22)	71.4 (10/14)	83.3 (30/36)	83.3 (20/24)	83.3 (10/12)
≦0.98	**95.5 (21/22)**	**71.4 (10/14)**	**86.1 (31/36)**	**84.0 (21/25)**	**90.9 (10/11)**
≦0.99	95.5 (21/22)	64.3 (9/14)	83.3 (30/36)	80.8 (21/26)	90.0 (9/10)
≦1.00	95.5 (21/22)	64.3 (9/14)	83.3 (30/36)	80.8 (21/26)	90.0 (9/10)

Data in parentheses are the number of cases used to calculate the percentages.

Table 5. Statistical data for the predicting malignancy with WLR fit

Threshold value of ADC ($\times 10^{-3}$ mm^2/sec)	Sensitivity (%)	Specificity (%)	Accuracy (%)	PPV (%)	NPV (%)
≦1.21	86.4 (19/22)	85.7 (12/14)	86.1 (31/36)	90.5 (19/21)	80.0 (12/15)
≦1.22	90.9 (20/22)	85.7 (12/14)	88.9 (32/36)	90.9 (20/22)	85.7 (12/14)
≦1.23	**90.9 (20/22)**	**85.7 (12/14)**	**88.9 (32/36)**	**90.9 (20/22)**	**85.7 (12/14)**
≦1.24	90.9 (20/22)	85.7 (12/14)	88.9 (32/36)	90.9 (20/22)	85.7 (12/14)
≦1.25	90.9 (20/22)	78.6 (11/14)	86.1 (31/36)	87.0 (20/23)	84.6 (11/13)

Data in parentheses are the number of cases used to calculate the percentages.

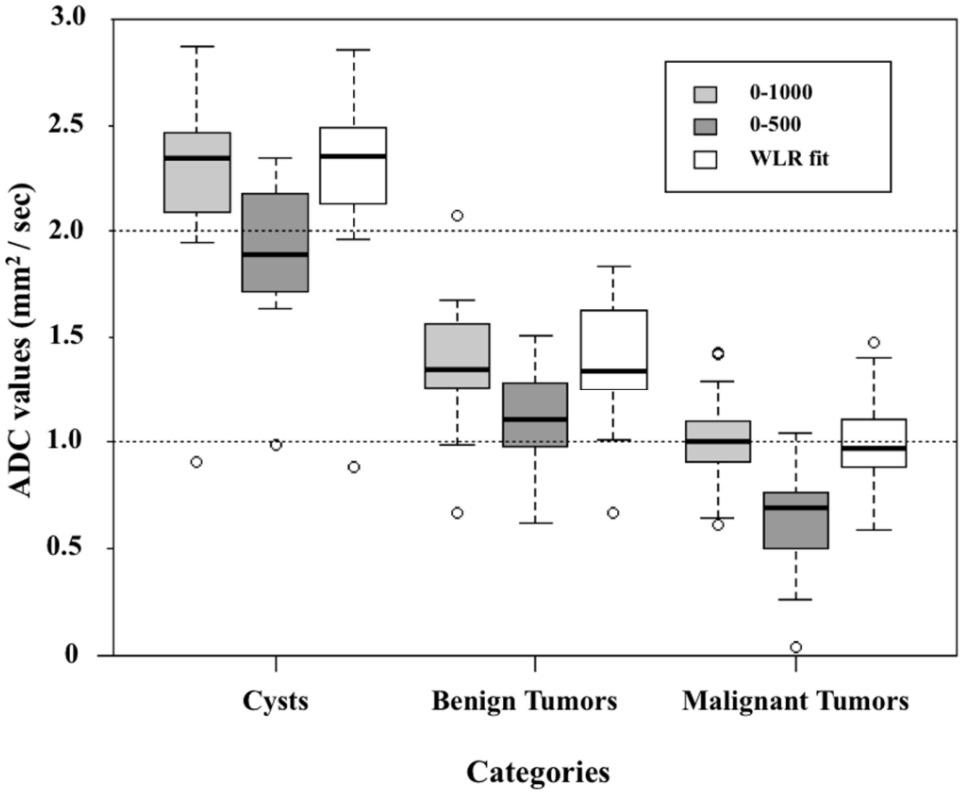

Fig. 1.
Box plots of ADC values with 0-1000 method (light gray boxes), 500-1000 method (gray boxes), and weighted linear regression (WLR) fit (white boxes) among three categories. Highest mean ADC value was that for cysts, followed by that for benign and malignant tumors with each method.

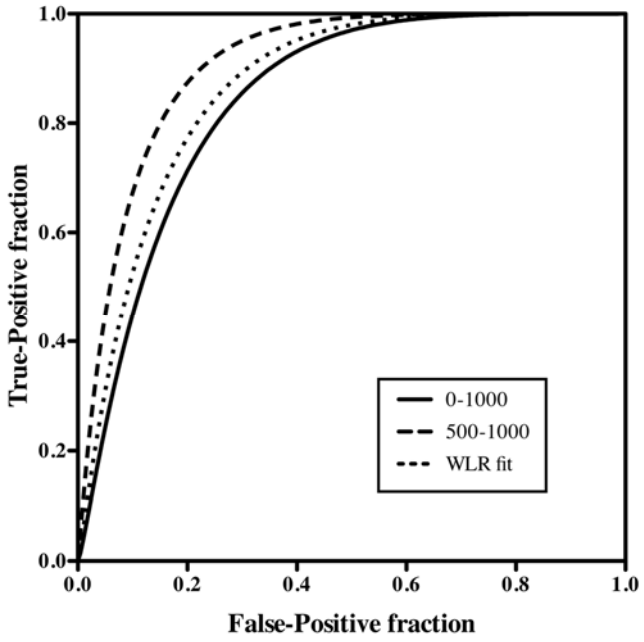

Fig. 2.
ROC curves of diagnostic ability for predicting malignancy among three methods for ADC measurement. Solid line indicates ROC curve with 0-1000 method; dashed line indicates that with 500-1000 method; dotted line indicates that with WLR fit.

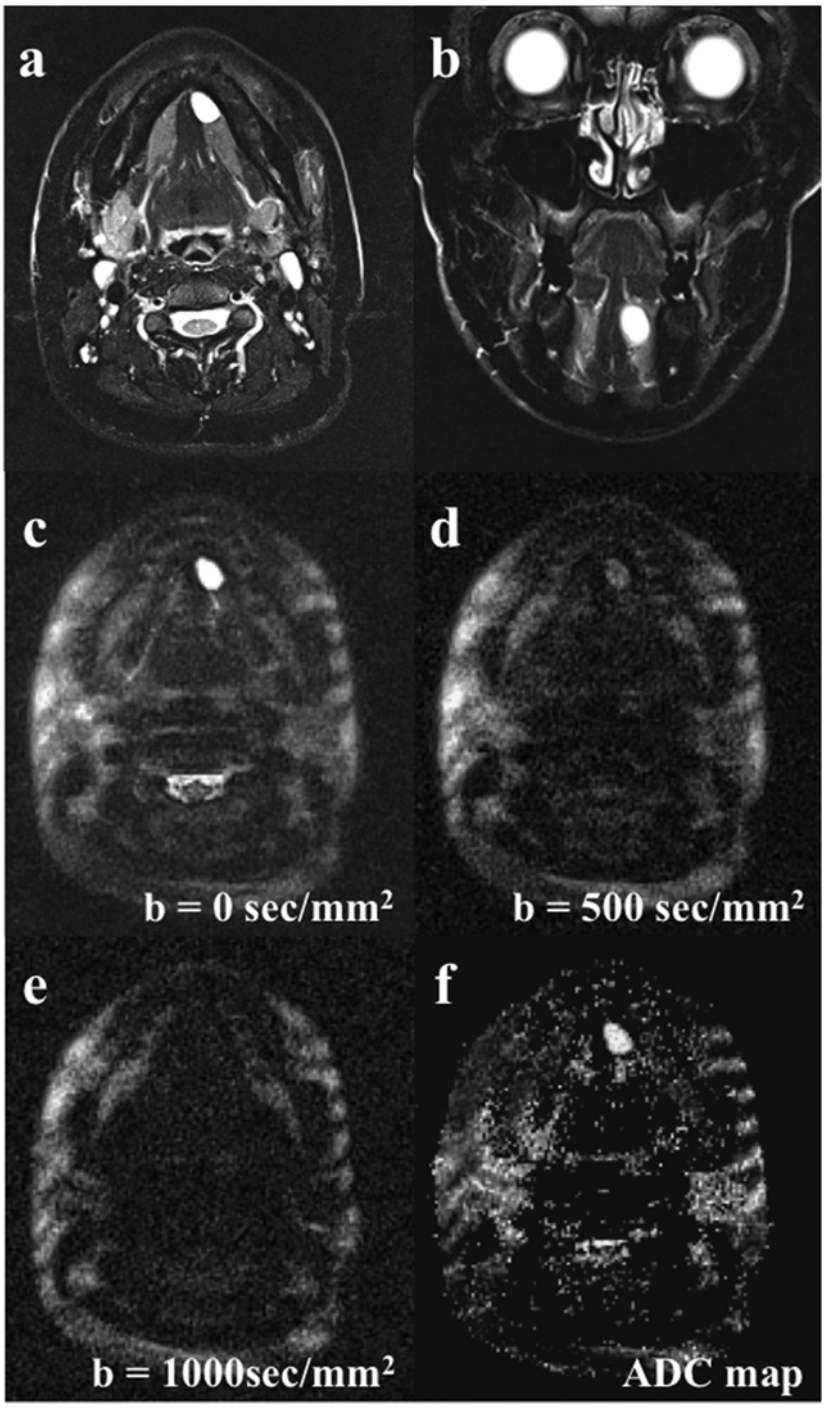

Fig. 3.
Ranula in left sublingual space in 20-year-old woman. (a)-(b) Transverse and coronal T2-weighted images with Dual-FS-STIR-CHESS revealed mass lesion with homogeneous, very high signal intensity. (c) HASTE DW MR image obtained with gradient b factor of 0 sec/mm^2 revealed mass lesion with very high signal intensity. (d)-(e) HASTE DW MR images obtained with gradient b factors of 500 and 1000 sec/mm^2 showed marked decrease in signal intensity of mass lesion. (f) ADC map shows that mass lesion had high ADC value of 2.09 × 10^{-3} mm^2/sec with 0-1000 method, 1.73 × 10^{-3} mm^2/sec with 500-1000 method, and 2.13 × 10^{-3} mm^2/sec with WLR fit. This case was correctly diagnosed as a non-malignancy using threshold ADC values with each method.

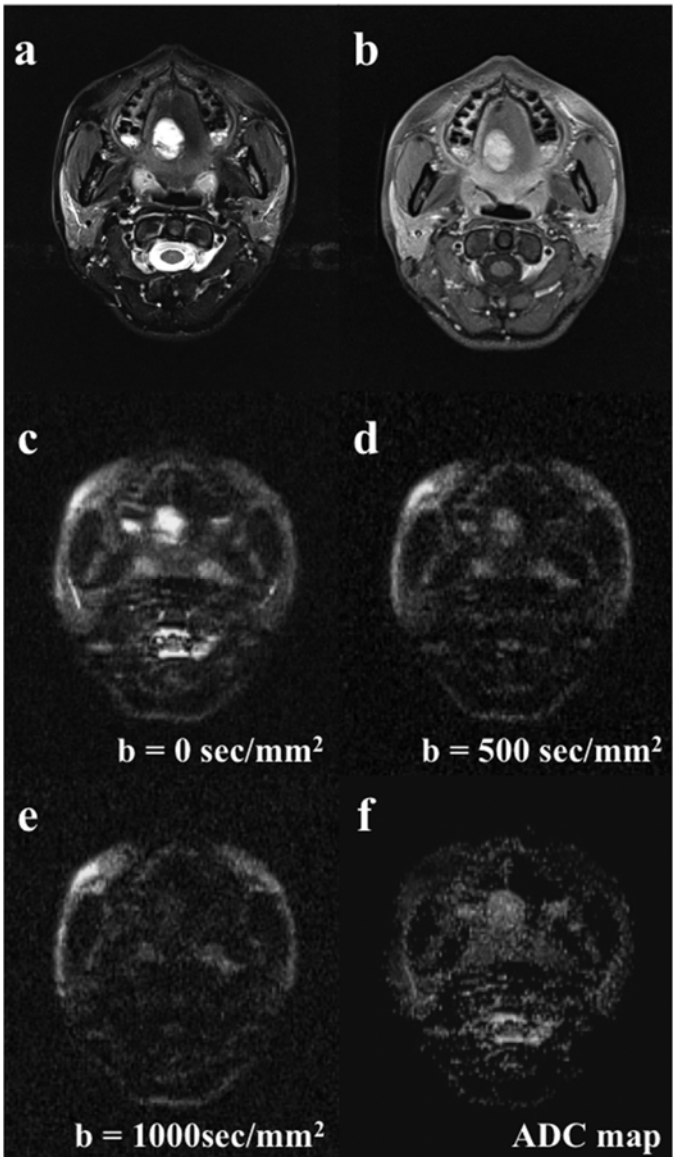

Fig. 4.
Myoepithelioma in right palate in 50-year-old woman. (a) Transverse T2-weighted image with Dual-FS-STIR-CHESS revealed mass lesion (arrowhead) with heterogeneous, very high signal intensity. (b) Transverse post-contrast T1-weighted image with fat suppression by CHESS showed mass lesion was enhanced strongly. (c) HASTE DW MR image obtained with gradient b factor of 0 sec/mm^2 revealed mass lesion (arrowhead) with very high signal intensity. (d)-(e) HASTE DW MR images obtained with gradient b factors of 500 and 1000 sec/mm^2 showed mild decrease in signal intensity of mass lesion. (f) ADC map shows that mass lesion had an ADC value of 1.54 × 10^{-3} mm^2/sec with 0-1000 method, 1.38 × 10^{-3} mm^2/sec with 500-1000 method, and 1.67 × 10^{-3} mm^2/sec with WLR fit. Whereas it is a little difficult to diagnose a mass lesion as a benign tumor using only conventional MR images, ADC values with HASTE DW imaging were very helpful in differentiating non-malignancy from malignancy in this case. This case was correctly diagnosed as a non-malignancy using threshold ADC values with each method.

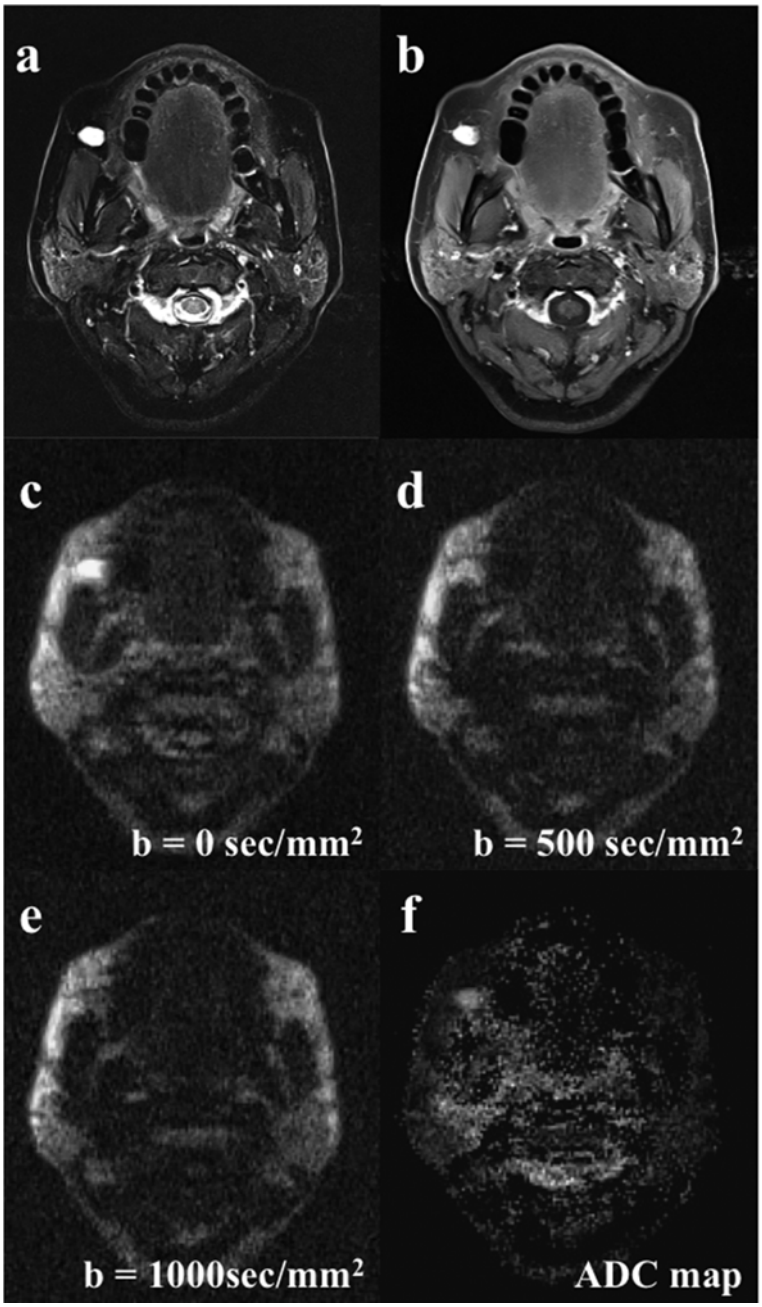

Fig. 5.
Cavernous hemangioma in right buccal space in 58-year-old woman. (a) Transverse T2-weighted image with Dual-FS-STIR-CHESS revealed relatively small mass lesion with homogenous, very high signal intensity. (b) Transverse post-contrast T1-weighted image with fat suppression by CHESS showed mass lesion was enhanced strongly. (c) HASTE DW MR image obtained with gradient b factor of 0 sec/mm^2 revealed mass lesion with very high signal intensity. (d)-(e) HASTE DW MR images obtained with gradient b factors of 500 and 1000 sec/mm^2 showed mild decrease in signal intensity of mass lesion. (f) ADC map shows that mass lesion had an ADC value of 1.46 × 10^{-3} mm^2/sec with 0-1000 method, 1.10 × 10^{-3} mm^2/sec with 500-1000 method, and 1.45 × 10^{-3} mm^2/sec with WLR fit. This case was also correctly diagnosed as a non-malignancy using threshold ADC values with each method.

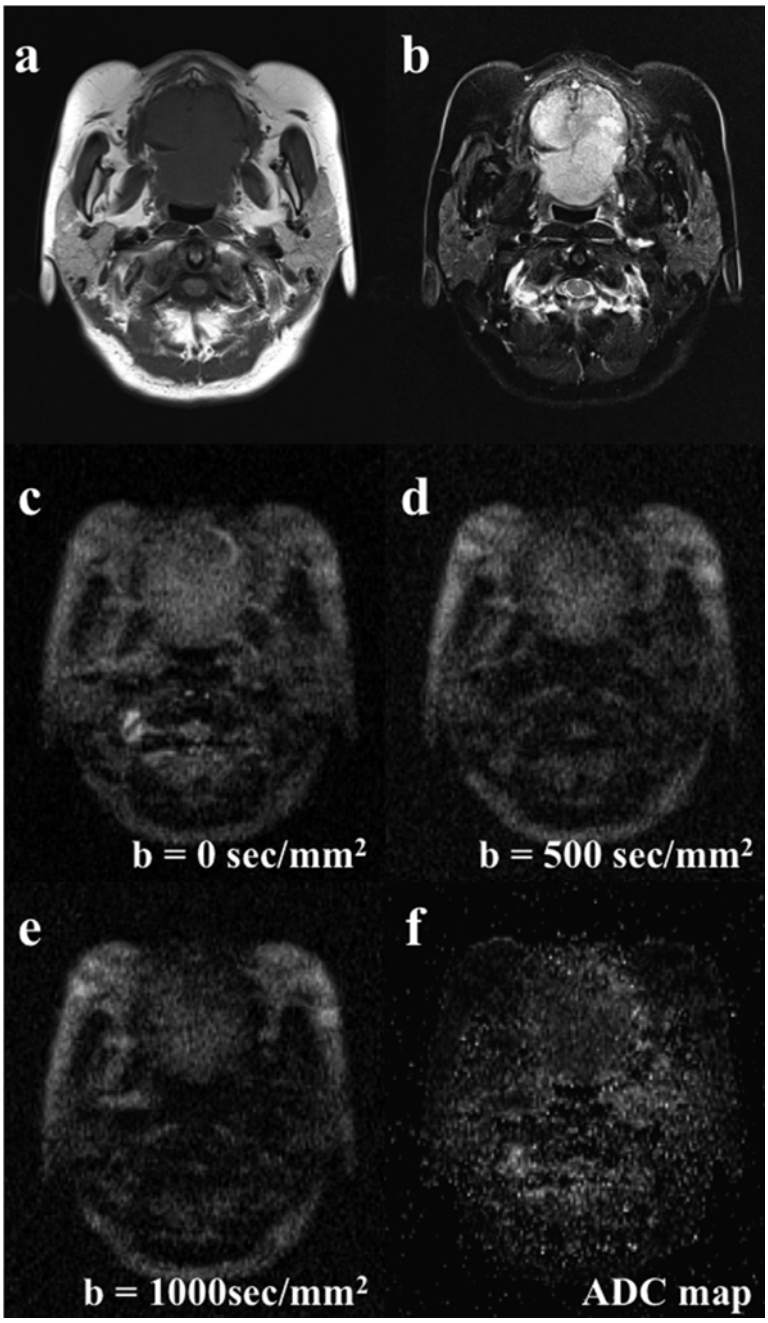

Fig. 6.
Malignant lymphoma in palate of 72-year-old woman. (a) Transverse T1-weighted image revealed mass lesion with homogeneous, low signal intensity. (b) Transverse T2-weighted image with Dual-FS-STIR-CHESS revealed mass lesion with homogeneous, slightly high signal intensity. (c) HASTE DW MR image obtained with gradient b factor of 0 sec/mm^2 revealed mass lesion with slightly high signal intensity. (d)-(e) HASTE DW MR images obtained with gradient b factors of 500 and 1000 sec/mm^2 showed slight decrease in signal intensity of mass lesion. (f) ADC map shows that mass lesion had relatively lower ADC value of 0.61 × 10^{-3} mm^2/sec with 0-1000 method, 0.49 × 10^{-3} mm^2/sec with 500-1000 method, and 0.59 × 10^{-3} mm^2/sec with WLR fit. This case was correctly diagnosed as a malignancy using threshold ADC values with each method.

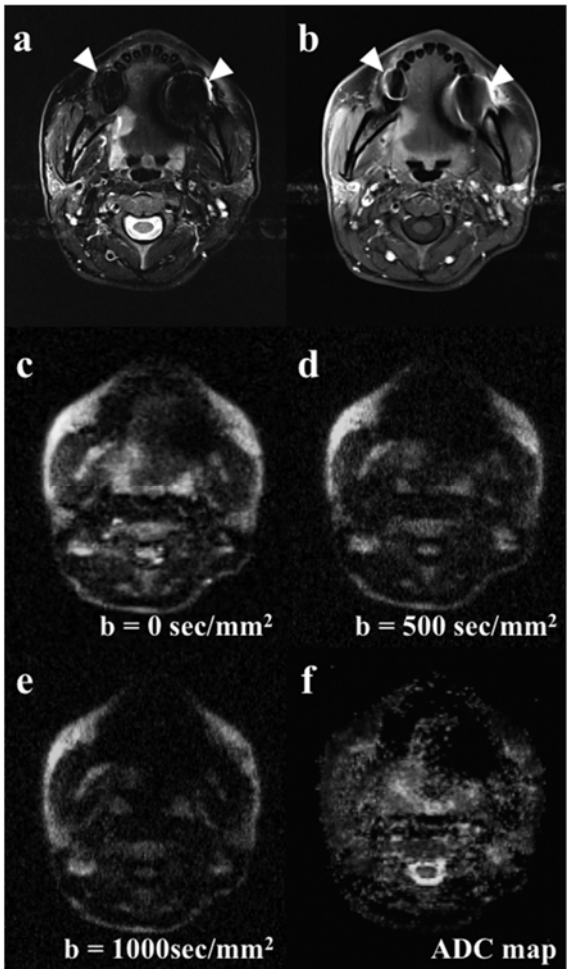

Fig. 7.
Squamous cell carcinoma in right tongue of 46-year-old woman. (a) Transverse T2-weighted image with Dual-FS-STIR-CHESS revealed mass lesion with high signal intensity. Susceptibility artifacts due to dental restorations (arrowheads) are shown on images. (b) Transverse post-contrast T1-weighted image with fat suppression by CHESS showed mass lesion was enhanced. Susceptibility artifacts due to dental restorations (arrowheads) are also shown on images. (c) HASTE DW MR image obtained with gradient b factors of 0 sec/mm^2 revealed mass lesion with slightly high signal intensity. Although susceptibility artifacts due to dental restorations were present on this image, as well as on T2-weighted images with Dual-FS-STIR-CHESS and post-contrast T1-weighted images with fat suppression by CHESS, no distortion severe enough to hamper ADC measurement was observed. (d)-(e) HASTE DW MR images obtained with gradient b factors of 500 and 1000 sec/mm^2 showed slight decrease in signal intensity of mass lesion. (f) ADC map shows that mass lesion had low ADC value of 1.00 × 10^{-3} mm^2/sec with 0-1000 method, 0.69 × 10^{-3} mm^2/sec with 500-1000 method, and 0.96 × 10^{-3} mm^2/sec with WLR fit. This case was also correctly diagnosed as a malignancy using threshold ADC values with each method.